Global observations of the zonal drift speed of equatorial ionospheric plasma bubbles

T. J. Immel, H. U. Frey, S. B. Mende, E. Sagawa

Annales Geophysicae (2004) 22: 3099–3107
SRef-ID: 1432-0576/ag/2004-22-3099

Annales Geophysicae

Global observations of the zonal drift speed of equatorial ionospheric plasma bubbles

T. J. Immel[1], **H. U. Frey**[1], **S. B. Mende**[1], **and E. Sagawa**[2]

[1]Space Sciences Laboratory, University of California Berkeley, USA
[2]Communications Research Laboratory, Tokyo, Japan

Received: 3 October 2003 – Revised: 31 January 2004 – Accepted: 9 February 2004 – Published: 23 September 2004

Part of Special Issue "Equatorial and low latitude aeronomy"

Abstract. Space-based measurements from an imager aboard the high-apogee NASA-IMAGE satellite allows for global-scale observations of nightside ionospheric densities and structure. Such a view cannot be provided by imagers in near-Earth orbit or based on the ground. The IMAGE Spectroscopic Imager (SI) isolates the Far-ultraviolet (FUV) O I 135.6 nm emission which is produced through radiative recombination of O^+. These observations clearly show the distribution of FUV emissions of the equatorial airglow bands over the range of local times between the evening terminator to points well after midnight. Determination of plasma drift speeds in these local time sectors is performed by identification and subsequent tracking of localized depressions in the FUV emissions. This determination is made for nearly 200 plasma bubbles in the March-May period of 2002. Important findings of this study include (1) an unambiguous association between D_{st} and zonal plasma drift speeds, and (2) a longitudinal dependence of the zonal plasma drift speeds, with a peak around the Indian sector. The first effect is attributed to penetrating ring current electric fields, while the second is apparently due to a longitudinal variability in the vertical polarization electric fields that directly affects the zonal plasma drift speeds.

Key words. Ionosphere (Equatorial ionosphere, Electric fields and currents, Ionosphere-magnetosphere interactions, Ionospheric irregularities)

1 Introduction

Recent studies of the nightside equatorial ionosphere demonstrate the utility of global-scale far-ultraviolet (FUV) imaging for retrieving important ionospheric parameters. Using global-scale images of the far-ultraviolet emissions produced by recombination of ionospheric O^+, Immel et al. (2003) and Sagawa et al. (2003) found that plasma drift speeds in the ionospheric anomalies could be determined through analysis of multiple successive images of the equatorial airglow bands. Such a determination depends on the presence of embedded brightness irregularities, a requirement easily fulfilled by the presence of equatorial ionospheric bubbles. Once produced in the post-sunset equatorial ionosphere, plasma bubbles appear as localized decreases in airglow brightness and can be tracked across the nightside to determine their zonal drift speed. Under the assumption that these depletions are embedded in the surrounding plasma, one can equate the bubble drift speed with the drift of the ambient ionospheric plasma (Mendillo and Baumgardner, 1982; Taylor et al., 1997; Pimenta et al., 2003).

In the above noted study, Immel et al. (2003) determined the globally averaged speed of zonal plasma drifts from IMAGE/FUV images of the O I 135.6 nm emission during March-May 2002. These were compared to zonal drifts determined by the Jicamarca radar from data obtained over several years (Fejer et al., 1991), whereupon it was determined that the global-averaged zonal drifts in the equatorial ionospheric anomaly were generally higher than those measured at the magnetic equator, especially at early local times. This latitudinal shear effect was noted earlier by Aggson et al. (1987), using in-situ plasma drift observations by the polar-orbiting DE-2 satellite. Recent studies confirm and help to explain this observation (Martinis et al., 2003), as F-region drifts have a stronger initial effect on plasma flux tubes that terminate in the anomalies than on plasma in flux tubes that terminate closer to the equator (with lower apex altitudes).

The current study is an extended investigation of the plasma drifts observed in the aforementioned year 2002 period. Of particular interest is the global distribution of plasma drift speeds, and the factors that may influence or cause systematic localized or global variability in these drift speeds. The significant variations in magnetic field strength, declination, and geographic latitude along the magnetic equator are factors that may well have (heretofore unobserved) localized effects on plasma drift speeds and the ionosphere in general.

Correspondence to: T. J. Immel
(immel@ssl.berkeley.edu)

The zonal drift of equatorial ionospheric F-region plasma was first described by Woodman (1972), using measurements from the radar facility at Jicamarca, Peru. Since then, numerous studies of the dependence of the zonal plasma drift on neutral wind interactions, solar irradiance, and geomagnetic activity have been undertaken (e.g. Fejer et al., 1981, 1985, 1991; Fejer, 1993; Fejer and Scherliess, 1998; Sobral and Abdu, 1991; Sobral et al., 1999; Scherliess and Fejer, 1998; Valladares et al., 1996; de Paula et al., 2002). The work described in this report is the first space-based imaging study that addresses the topics previously studied using only ground-based or in-situ measurements.

Several studies have investigated the properties of the equatorial ionosphere with specific attention to longitudinal variations in the properties of the plasma. The global distribution of vertical plasma drifts was examined by Fejer et al. (1995), using data from the AE-E satellite. However, AE-E only measured cross track drifts, and given its low-inclination orbit ($\sim$19°), the zonal speeds were generally along the satellite track and not unambiguously separable from the satellite velocity. Coley et al. (1994) did look at the global distribution of low-latitude zonal plasma drifts from the polar-orbiting DE-2 satellite, but as a function of local time rather than longitude. In an earlier study of DE-2 data, Coley and Heelis (1989) state that aside from a somewhat different strength and location of the evening zonal drift reversal, the zonal drifts do not depend on longitude. Maynard et al. (1995) performed a thorough analysis of low-latitude drift velocities measured by the San Marco D satellite, showing the variability as a function of solar radio flux, lunar phase, season, and longitude. While the zonal plasma drifts showed little variation with longitude, it was found that the vertical drifts had a significant longitudinal dependence, with a maximum dayside vertical drift speed in the Indian sector. The San Marco D satellite had the lowest inclination of all the satellites discussed here ($\sim$3°).

This research aims to provide a new and comprehensive set of observations of low-latitude plasma drift speeds over several months of time between equinox and solstice. In particular, the goal is to determine the degree of influence of factors such as magnetic activity, solar output, or geographic location. The IMAGE/FUV data set provides a unique global view with simultaneous measurements over $>$90° of longitude, and continuous, extended ($>$5 h) observations of changes in densities in the low-latitude ionospheric anomalies, including individual plasma bubbles. Its utility in making ionospheric observations should prove to benefit the understanding of the physical processes influencing the low-latitude ionosphere.

2 Instrumentation: IMAGE/FUV SI-13

The NASA-IMAGE satellite was placed into a highly elliptical polar orbit by a Boeing Delta II launch vehicle on 25 March 2000. Apogee was originally at 40° north latitude, but through apsidal motion the apogee reached 90° N in 2001, and by March 2002 was again approaching 40° N latitude, with right ascension of apogee 180° away from the initial orbit. The low latitude of apogee in 2002 provided observation times well suited for equatorial measurements. The orbital geometry was equally favorable at the beginning of the mission, but the imager was operated primarily as a high-latitude auroral imager at that time. The focus of this study remains, therefore, on the 2002 observations.

The Spectrographic Imager (SI) on board IMAGE has two FUV wavelength channels, one to obtain images of Doppler-shifted hydrogen emissions at 121.8 nm, originating in the proton aurora, and another to spectrally separate and obtain images of the 135.6 nm emission of O I (Mende et al., 2000). In the terrestrial environment, this emission of O I generally has two causes; either excitation by impact of energetic electrons produced by solar Extreme-ultraviolet (EUV) photoionization or ionization through precipitation of auroral particles, or by radiative recombination of ionospheric O^+. The later reaction is also responsible for the 630.0 and 777.4 nm emissions often observed by ground-based observers at equatorial or mid-latitude stations (Weber et al., 1978; Meriwether et al., 1985; Makela et al., 2001).

The 135.6 nm channel of the SI is usually called SI-13. The SI-13 is insensitive to the bright, optically thick emissions of O I at 130.4 nm, though with its 5-nm passband centered at 135.6 nm it is sensitive to a particular N_2 Lyman Birge Hopfield (LBH) band emission at 135.4 nm. For observations of the aurora or the daytime airglow this must be taken into consideration. However, in the nighttime middle-to-low latitude ionosphere, the LBH emission is basically absent, and the signal in the SI-13 is purely due to the 135.6 nm emissions. Final stellar calibrations (Frey et al., 2003) report an instrumental sensitivity of 15.3 counts per 1000 Rayleighs (R) per pixel (5-s exposure) of O I 135.6 nm emissions. The counting rates for observations in the equatorial ionospheric anomaly regions generally peak around 5–8 counts per pixel, indicating emissions less than 500 R, close to the expected brightness.

With a 14.2-h orbit period, the imager can dwell on low-latitude emissions for 6–8 h per orbit. As shown by Immel et al. (2003), the duration of the observation is sufficient to observe any significant changes in the brightness and/or morphology of the emissions originating in the ionospheric anomaly. Though the images are global in scale, the latitude of apogee in the March-May 2002 time of interest is not ideal for observations of the southern anomaly, or even of the northern anomaly in regions where the magnetic equator dips well into the Southern Hemisphere (i.e. South America). The combination of this fact and a known seasonal reduction in the occurrence of spread-F and ionospheric bubbles in the South American sector beginning in April-May (Valladares et al., 1996) result in a total lack of bubble observations over 70° of longitude in the South American sector for the 2002 observational season.

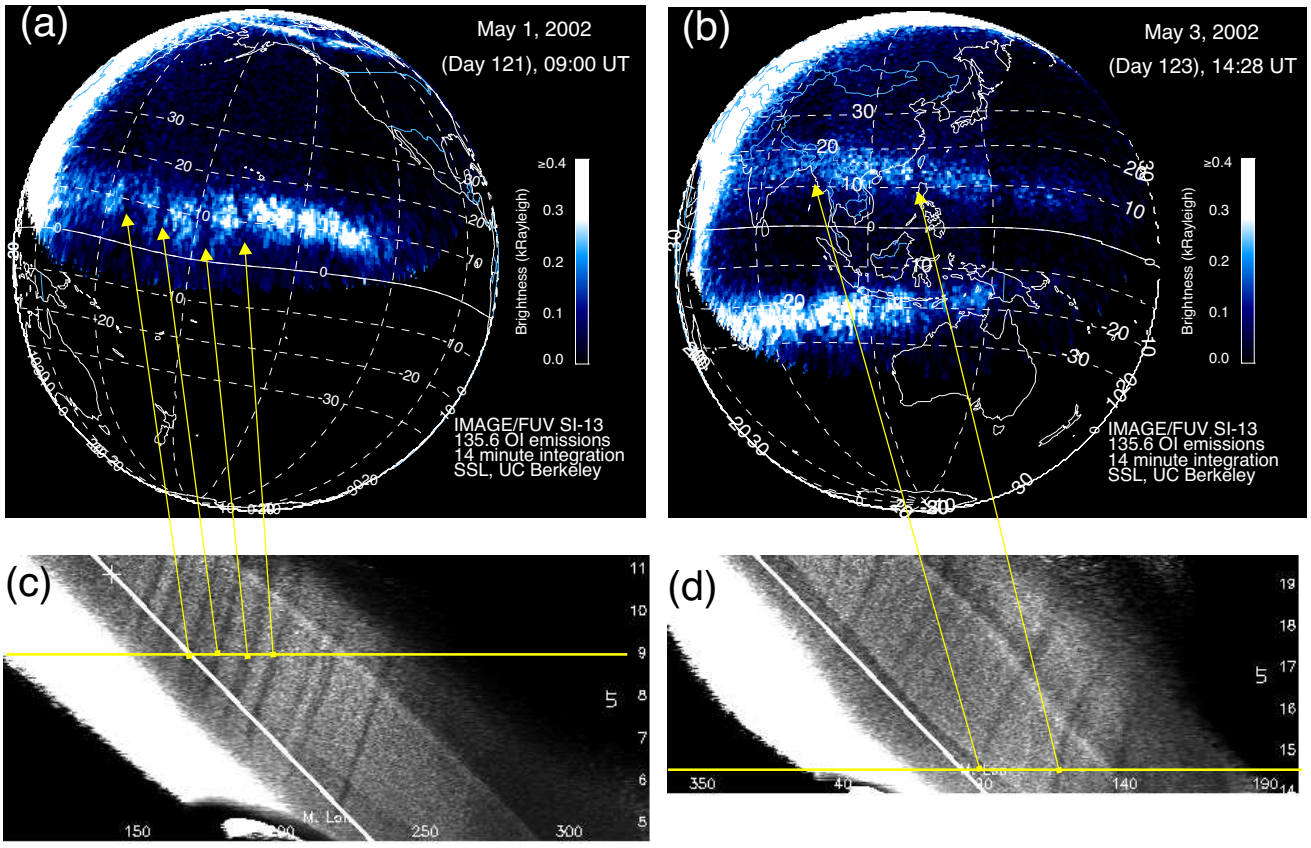

Fig. 1. Two 135.6 nm imaging examples with keograms of integrated brightness. Figures 1**a**, **b** show images resulting from integrations of seven 5-second SI-13 exposures obtained during 14 min of nominal imager operations with 2-min imaging cadence. These are mapped onto a projection of geographic coordinates centered at 22:00 LT on days 121 and 123 of 2002, respectively. Figures 1**c**, **d** show keograms of the latitudinally integrated brightness in the northern airglow band for a period of observations including the images shown above. The horizontal scale of the keograms indicates magnetic longitude, where 0° longitude coincides with Greenwich, and the vertical scale indicates UT. The time of the image is indicated with a horizontal yellow line and the features in the images associated with depletions in the keogram are noted with arrows.

3 Data analysis

3.1 Determination of drift speeds, two examples

Figure 1 shows a pair of images from early May 2002, mapped to an orthographic projection of geographic coordinates with contours of magnetic latitude and longitude superposed. The center of the projection is at the geographic equator and 22:00 LT. The upper left image is the average brightness observed in 7 successive images (obtained over 14 min) from the SI-13 instrument, beginning at 09:00 UT on 1 May. The upper right image is a similar projection of the average of 7 successive images obtained after 14:28 UT on 3 May. Each of these images shows the emissions from the northern equatorial airglow band, that extend from the region of bright airglow at the western edge of the disc across the nightside. The 3 May image also shows the southern airglow band, whose brightness is enhanced due to the effect of limb brightening, as the southern band was near the imaging horizon at this time.

Each of these images is obtained at a time during which several low-latitude ionospheric plasma bubbles are generated and proceed to drift across the nightside. Below each image is a record of the latitudinally-integrated brightness of the northern airglow band as a function of magnetic longitude and UT. Every image is processed and represented as a single row of pixels in this keogram. A horizontal yellow line underlies the row of pixels corresponding to the above image. The vertical scales are identical so the vertical size of the keogram is representative of the total time of observation. In each keogram, airglow depletions associated with plasma bubbles appear as dark stripes, depressions in brightness which drift eastward with time. The depletions can also be seen in the images, and the locations of the bubbles in the images are identified by arrows originating at their corresponding location in the keograms. The white line in the keograms indicates the motion of the location of 20 h Magnetic Local Time (MLT) in the keogram.

The 1 May case shows several well-defined, localized depletions in airglow brightness. Four plasma bubbles are

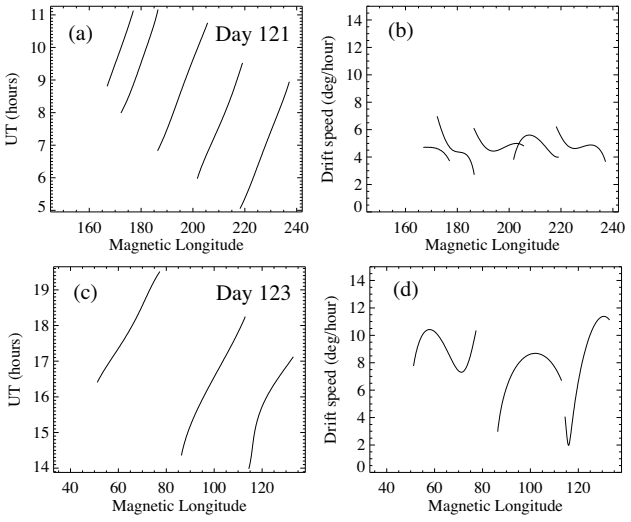

Fig. 2. Locations and velocities of major brightness depletions from keograms of Fig. 1. (**a**) The locations of 5 brightness decreases seen in the keogram of Fig. 1c are determined and plotted as a function of MLon vs. UT. (**b**) The drift speed of each depletion shown in 2a is shown as a function of MLon. (**c**, **d**) These panels repeat the presentation of 2a, b, but following three brightness depletions from Fig. 1d.

clearly identifiable in the image and in the keogram. The 3 May case does not have such strong depletions, but the locations of two depletions can still be identified in both the keogram and the image. A comparison of these keograms reveals that the 1 May depletions show a much more steady drift across the nightside than the 3 May case, when the drifts are more variable and often more rapid.

Figure 2 shows the locations and speeds of the most easily identifiable bubbles. Figures 2a and 2b show the bubbles' positions and drift speeds, respectively, in Magnetic Longitude (MLon) vs. UT coordinates for the 1 May period of interest. The positions (longitudes) are determined for each row of the keogram from a Gaussian function least-squares fitted to the brightness vs. ML on data around the position of the bubble. The initial position is determined by hand, then determined by a Gaussian fitting of a 13-point subset of the row of counts centered on the last observed position of the depletion for all subsequent points. If the fitting procedure fails to converge to a solution, the position of the minimum counting rate is used. The speeds are determined using a 4th degree polynomial, least-squares fitted to the position of each plasma bubble vs. UT (as shown in Fig. 2a). The derivative of this fit, i.e. the fitted speed of the plasma bubble, v, is determined. These plots show that the 1 May period exhibited several bubbles between geomagnetic longitudes 160° and 240°, drifting at speeds of around 5°/hour, on average. The low rate of change in drift speeds seen in the 1 May keogram (Fig. 1c) is reflected here in the velocity plot.

The 3 May locations and velocities are shown in Figs. 2c and 2d, respectively, showing finally the velocities of three plasma bubbles observed between 50° and 130° MLon. The westernmost bubble displays variability similar to that seen on 1 May, with a peak speed of 10°/hour around 50 MLon, with gradually slowing speeds afterwards. The next bubble to the east shows a general increase in velocity from 3° to 9°/hour between 85° and 102° MLon, followed by a slowdown back to ∼6 m/sec around 115°. The easternmost bubble shows only a consistent increase in velocity between 115° and 138° MLon.

These later bubble drifts conflict with the generally observed variation, that nightside plasma drift speeds slow with local time (Fejer et al., 1991). The reason for this variation and the significant difference between the day 123 and 121 plasma drifts is not clear from the images, as in each case the airglow bands are nominally located around ± 10–15° magnetic latitude, and the level of magnetic activity is about the same on the two days (average $K_{p121}(D_{st121})$= 1.3 (5 nT) vs K_{p123} (D_{st123})= .9 (1.3 nT)). The most obvious difference between the two observations is that the drifts are being measured over different parts of the Earth, separated by 100° of longitude. Whether the drift speed behavior observed on day 123 is unique to this imaging time/geographic sector or is observed more frequently will be investigated in the course of this study.

3.2 Relation of drift speeds to magnetic and solar activity

3.2.1 K_p and D_{st} dependences

Before analyzing the data for any global variations in drift speed, other influencing factors must be determined, and if necessary, removed from the data set or otherwise accounted for. One area of interest is the effect of magnetic activity on low-latitude electric fields, that will in turn affect the plasma drift speeds observed.

There are a total of 104 plasma depletions observed during the days between 87–129, 2002 that are tracked to determine drift speeds. The level of magnetic activity during these times is such that most bubbles are seen to occur during periods of low-to-moderate activity, where $K_p \leq$ 3+. Several bubbles were seen around the time of the 17–21 April storm period, where K_p was in the range of 4–6. These are the only observations at high levels of activity, however, which may be too few for a good statistical analysis of the effects of high magnetic activity.

To determine any possible effect of geomagnetic activity on plasma drift speeds, the drift velocities are determined for all bubbles as described in the previous section. The MLT of the bubble and the magnetic planetary K index (K_p) at each imaging time is recorded along with the velocity, and the average velocity is determined in one hour bins of MLT, and in bins of K_p, where, for example, K_p=3$^-$, 3^o and 3$^+$ are considered equivalent. The average drift speed as a function of K_p can therefore be plotted in separate bins of MLT, as shown for six MLT bins in Fig. 3. In these panels, heavy diamonds indicate values for which the standard deviation of the mean velocity (σ_m) is <50% of the actual value. The dotted lines indicate the envelope of these standard deviations.

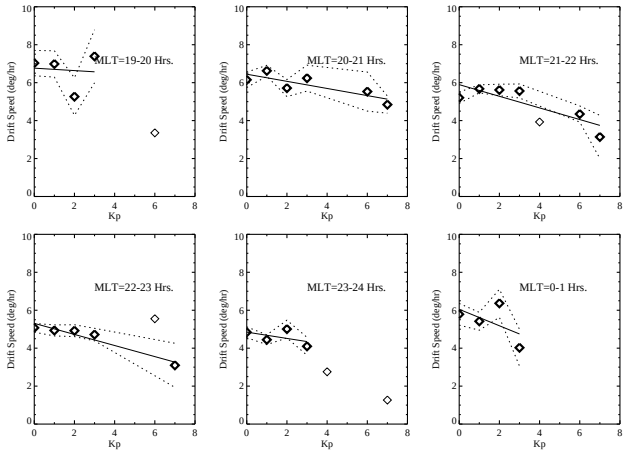

Fig. 3. K_p dependence of the drift speeds in 6 magnetic local time sectors. In each plot, the most statistically significant points are shown with heavy diamonds and error bars. Less significant points are shown with light diamonds and no error bar. A linear least-squares fit is calculated and overlaid in each panel. The average coefficient of linear correlation over these six magnetic local time sectors is 0.63.

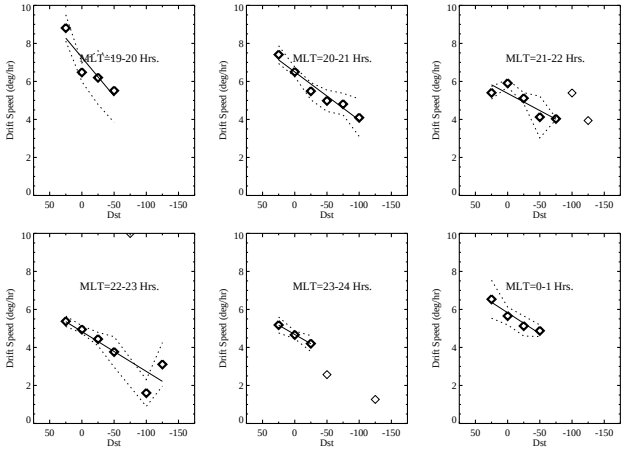

Fig. 4. D_{st} dependence of the drift speeds in 6 magnetic local time sectors. As in Fig. 3, the most statistically significant points are shown with heavy diamonds and error bars. Less significant points are shown with light diamonds and no error bar. A linear least-squares fit is calculated and overlaid in each panel. The average coefficient of linear correlation over these six magnetic local time sectors is 0.93.

Light diamonds are points where σ_m is greater than 50% of the speed, though these standard deviations are not shown.

Each frame of Fig. 3 shows a slightly different variation in drift speeds vs. K_p, but the trend towards lower values with increasing K_p is clear in the 20:00–23:00 MLT range. Inclusion of the high standard deviation points would extend the trend to 19:00–24:00 MLT. In each panel, a line is least-squares fitted to the points represented by the heavy diamonds. The average of the coefficients of linear correlation is -0.63. This is a fair correlation, and shows a significant relation between drift speeds and K_p.

A similar analysis is carried out using the geomagnetic storm index, D_{st}, as the indicator of magnetic activity. The average plasma drift speeds are now determined in one hour bins of MLT and 25 nT bins of D_{st}. The average speeds are shown in Fig. 4, where heavy and light diamonds again demark points with σ_m less or greater than 50% of the mean speed, respectively. This set of figures shows a very definite decrease in drift speed with decreasing D_{st} (increasing magnetic storm activity) across all local time sectors. Linear lines are fitted to the heavy diamonds (in a manner similar to that used for Fig. 3), and the average coefficient of linear correlation in the 06:00 MLT sectors is -0.93. This indicates an excellent correlation between the storm time ring current strength and the low-latitude zonal plasma drift speeds.

The result of this analysis is that any study of the longitudinal variation in drift speed must take into account the value of the D_{st} index, and either sort the data by that index or determine a correction factor to apply based on the value of D_{st}. The relation with K_p is noteable, but of lesser importance than D_{st}, and probably not causative. The linear fits shown in the D_{st} plots characterize the variation of the drift speed, and are used to develop correction factors that may be applied to any set of drift speed observations, to normalize the observed speeds to D_{st}=0 nT. From this point onward, all analyses are performed using drift speeds that are normalized to D_{st}=0 nT.

3.2.2 Solar 10.7 cm and EUV flux dependences

If the drift speeds measured by the FUV instrument are truly plasma drift speeds, a manifestation of the known relation between solar irradiance, zonal neutral winds and ion drifts should be revealed in an analysis of these data (Biondi et al., 1991, 1999; Fejer et al., 1991). Until the late 1980s, no consistent direct measure of solar EUV irradiance was available, but a good long-term correlation between the EUV flux and the 10.7 cm solar radio flux provided a ground-based and consistently measurable proxy for solar EUV. Consistent, direct measurements are now available, however, and the EUV fluxes in narrow (26–34 nm) and wide (1–50 nm) passbands have been provided by the SOHO-SEM instrument since the beginning of the NASA-IMAGE observations (Judge et al., 1998). Here, comparisons between each of these parameters and the measured plasma drift speeds are made in one hour bins of MLT, similar to the analyses of Section 3.2.1. As noted before, all of these data are normalized to D_{st}=0 nT in the manner described in Sect. 3.2.1.

To compare the plasma drift speeds and $F_{10.7}$, the average drift speeds are determined in 1 h bins of MLT and 25 Jansky (Jy) bins of solar radio flux. The results are shown for 6 bins of MLT in Fig. 5. Heavy (light) diamonds indicate values where σ_m was less (greater) than 50% of the mean, and $v \pm \sigma_m$ is indicated by dashed lines. In each panel, a linear fit to the data, weighted by the inverse of σ_m, is overlaid. In every case, this fit has a positive slope, indicating an observed

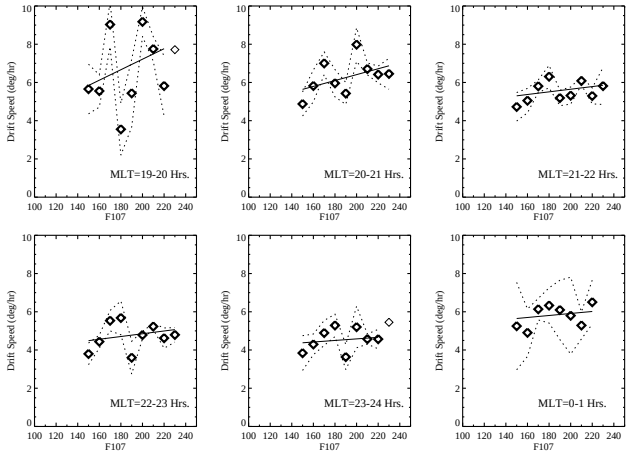

Fig. 5. $F_{10.7}$ dependence of the drift speeds in 6 magnetic local time sectors. As in Fig. 3, the most statistically significant points are shown with heavy diamonds and error bars. Less significant points are shown with light diamonds and no error bar. A linear least-squares fit is calculated and overlaid in each panel. The average coefficient of linear correlation over these six magnetic local time sectors is 0.34.

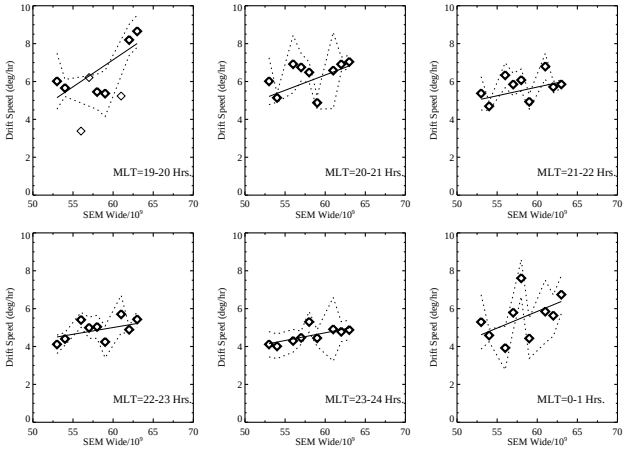

Fig. 6. Solar EUV flux dependence of the drift speeds in 6 magnetic local time sectors. As in Fig. 3, the most statistically significant points are shown with heavy diamonds and error bars. Less significant points are shown with light diamonds and no error bar. A linear least-squares fit is calculated and overlaid in each panel. The average coefficient of linear correlation over these six magnetic local time sectors is 0.56.

increase in drift speed with solar activity. The correlation of linear correlation is determined for each panel, the average of the 6 panels is 0.34. Though the correlation is not great, it indicates a moderate degree of confidence in the trend toward positive slopes suggested by each of the 6 separate fits.

Comparisons of the drift speed with solar EUV flux is done in a very similar manner as the previous analysis of the $F_{10.7}$ dependence. In this case, the data are binned in units of 10^9 photons/cm^2/sec, and in this case only the wide-band data are used. The range of solar fluxes over the period of interest is from 52–64 $\times 10^9$ photons/cm^2 sec. Unlike the $F_{10.7}$ measurement, the space-based detector is overwhelmed by energetic solar proton fluxes occurring during and after flares, so the days between 17–23 April 2002 are not included. The results of this analysis are shown for six MLT sectors in Fig. 6.

The overall increase in the zonal drift speed with increasing solar EUV flux is clear in each sector of MLT. Linear least-squares fits to the points represented by heavy diamonds all have a positive slope. The average coefficient of linear correlation is 0.56, which is not outstanding, but is more significant than the coefficient calculated in the above-performed $F_{10.7}$ analysis. This is expected, as the EUV flux directly affects thermospheric temperatures, pressure gradients, and in the end, zonal neutral winds and vertical electric fields. The $F_{10.7}$ is just a proxy for this, with a better correlation over longer terms than over periods of significant daily variation (as noted by Hedin (1984)), such as is the case in March–May 2003.

3.3 Longitudinal Drift Speed Variability

To this point, the approach has been to determine the influence of geophysically important effects through comparisons with magnetic and solar indices or measurements. The velocity measurements have been averaged in bins of these factors and MLT, with no regard to the terrestrial location of the measurement. In this section, the importance of terrestrial location is investigated. Using the results of the earlier sections, it is possible to remove geophysically controlled variability to better reveal geographic dependences. Though all of the comparisons yielded results of some significance, the D_{st} MLT analysis showed very significant linear correlations, from which correction factors for subsequent removal of the D_{st} effect are determined. Corrections for D_{st} effects have already been applied in Sect. 3.2.2, and are applied in this section as well.

The D_{st}-corrected plasma drift velocities are shown versus geomagnetic longitude in Fig. 7. In this case, as with the plots shown in Figs. 1 and 2, the 0° reference is a magnetic meridian through Greenwich. These velocities come from 4 separate one-hour bins of MLT, from 20:00 to 24:00 MLT, proceeding from the top to bottom panel. Each diamond represents the average speed of all bubbles observed in one-degree bins of MLon. Obvious is the gap in the South American sector, where bubbles are not observed during the entire observational period. In addition to the unfavorable seasonal effect, the number of observations in that sector is less, with only ∼2500 images containing pixels located at those longitudes vs. a peak imaging frequency of nearly 6000 during the same observation period (occurring around 120°). The seasonal effect is discussed at length by Valladares et al. (1996), while the later effect is due to observational geometry and the southward excursion of the magnetic equator in the South American sector.

Figure 7 shows that the drift speeds are not randomly distributed about a mean value, but in each MLT sector exhibit

a peak speed between 60 and 100°. In each MLT sector, this peak speed represents up to a 50% excursion away from the mean value. For instance, in the 20:00–21:00 MLT sector, after filtering the data with a 15° wide moving median function, the peak speed is 9.9°/h, while the mean speed is 6.5°/h. In that sector, this peak is located just to the west of the peak in the magnetic field strength in the anomaly (determined at 15° magnetic latitude using the IGRF reference field). Closer to midnight, the peaks in drift speed and magnetic field strength are nearly colocated.

4 Discussion

The first notable result of this research is the correlation between the solar radio flux and the low-latitude plasma drift speed, and the improved correlation when the speeds are compared directly to solar EUV flux. The covariation of drift speeds and solar indices has been noted in several research efforts (e.g. Sobral and Abdu, 1991; Fejer et al., 1991)) and is related to the increased thermospheric temperatures and pressure gradients resulting in higher neutral winds (Biondi et al., 1991). All of the studies cited here used the solar $F_{10.7}$ flux as a proxy for solar EUV, but also used data from events distributed through several years of time, taking advantage of the long-term correlation between EUV flux and $F_{10.7}$. In this study, the observations are distributed over only 2 months of very active solar activity, in which case it is better to compare to direct EUV measurements. This is clear from the high correlation between drift speeds and solar EUV flux, as compared to $F_{10.7}$.

A more significant result is the correspondence between zonal plasma drift speeds and D_{st}, where the eastward nighttime drifts slow with increasing level of disturbance (negative D_{st}). Compared to previous studies of the effect of magnetic activity on the low latitude ionosphere, this result is outstanding in several respects. Scherliess and Fejer (1997) found very good correlation between low-latitude vertical plasma drifts and the auroral electrojet index (AE), given a time delay on the order of several hours. This differs from our results as, (1) the AE and D_{st} indices measure completely separate (though related; see Kamide et al. (1998)) ionospheric and magnetospheric current systems, respectively, and (2) IMAGE/FUV provides zonal plasma drifts where Scherliess and Fejer (1997) analyzed the vertical plasma drifts provided by the Jicamarca radar. In this work, no analysis of the time delay between the D_{st} and drift speeds that results in the greatest correlation is reported, as the coefficient of linear correlation is already greater than 0.9, which is around the peak correlation found by Scherliess and Fejer (1997).

The slowing of zonal drifts in the vicinity of the ionospheric anomaly during heightened magnetic activity is often attributed, at least in part, to the perturbations to the global thermospheric wind system generated in response to increased high-latitude Joule heating. The wind perturbation generates electric fields that basically act to suppress the normal quiet-time ionospheric current system, an effect of

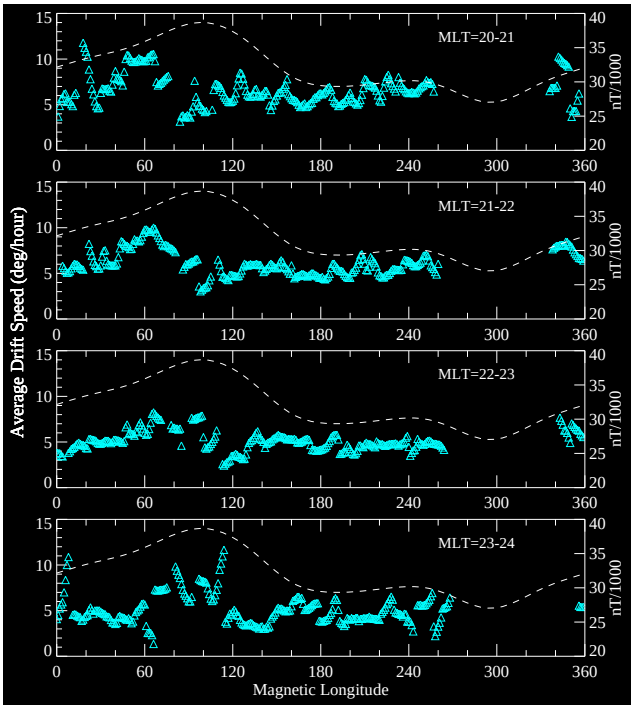

Fig. 7. Zonal drift speed vs. MLon in 4 Magnetic Local Time sectors. From top to bottom are shown the average plasma drift speed at all observed MLons in one hour bins from 20:00–24:00 MLT. Overlaid with a dashed line on each plot is the IGRF magnetic field strength at 15° in units of 1000 nT. The peak velocities are seen in the 60-100° MLon sector, with the peak shifting westward with increasing MLT.

which is the reduction of vertical low-latitude electric fields along with zonal neutral wind speeds (Blanc and Richmond, 1980). In this respect, it is even more interesting that the relation between D_{st} and zonal drift is so significant (much more so than the relation with K_p), as the disturbance dynamo is driven by high-latitude inputs, which are not measured by D_{st}. The close correspondence between v and D_{st} indicates an effect of electric fields originating in the ring current, with an influence at least as great as disturbance dynamo effects. The correspondence between zonal drift speed and D_{st} does not lend direct support to either the penetration of magnetospheric convection electric fields (Burke and Maynard, 2000; Fejer, 2002) or to the interplanetary electric field Kelley (1989) to low latitudes as the causative mechanism slowing the equatorial zonal plasma drifts. However, to the extent that enhancements in the ring current and D_{st} are driven by increased convection, we cannot rule out a slowdown in zonal drifts caused by penetrating convection electric fields as described by Fejer and Scherliess (1998).

The greatest storm-time penetration effects are usually manifested in vertical motion of equatorial plasma, or the imposition of a zonal electric field (Tanaka, 1986; Foster and Rich, 1998). The zonal plasma drift speed variation observed here suggests that a radial electric field, possibly originating in the enhanced ring current, is present in the equatorial F-

region. Such a source is described by Ridley and Liemohn (2002), where, in particular, the authors note the outward radial electric fields which develop on the nightside in response to enhancements in the region 2 current system occurring under magnetic storm conditions. Their simulation work predicts outward radial electric fields at ∼3000 km altitude of 2–10 mV/m during magnetic storms, with D_{st} ranging from −50 to −200 nT. The penetration of only a small percentage of the maximum value of 10 mV/m down to the F-region of the ionosphere would be sufficient to slow the zonal drifts to the degree seen in Fig. 4. That work also attributes the low-latitude penetration of magnetospheric electric fields to the addition of ring current polarization electric fields to the convection electric fields, a result also described in earlier research efforts (e.g. Blanc, 1978). It may well be that the zonal drift speed vs. D_{st} relationship described in Sect. 3.2.1, which is here attributed to ring current enhancement, describes the same reduction of low-latitude plasma drifts noted by Fejer and Scherliess (1998) during periods of enhanced magnetospheric convection.

The reason for the overall longitudinal enhancement in drift speeds in the South-Southeast Asian sector is less clear. From a simple view of the physics of the low-latitude ionosphere where the drift speed is proportional to |E|/|B|, this result is not expected. A maximum in the magnetic field should generally result in a minimum in the $\mathbf{E}\times\mathbf{B}$ drift speed. These data suggest that some process is at work to cause the vertical electric fields to reach large values in this sector exceeding the ∼30% heightening of the magnetic field. One cause of this could be very low Pedersen conductivities in this sector. This could be a result of a localized enhancement in the daytime equatorial fountain, an effect noted by Maynard et al. (1995). The stronger evacuation of ionospheric plasma would lead to reduced low-latitude plasma densities in the afternoon sector, which would corotate to the nightside. Another possibility is that the integrated effect of thermospheric neutral winds on the ionosphere leads to higher drift speeds in this sector. This would occur if in this longitude sector the influence of neutral winds at F-region altitudes is greater influence than in the E-region relative to other locations on Earth. This requires that a larger proportion of plasma along an ionospheric flux tube lie above the E-region, which could also result from an enhanced daytime uplift of the ionosphere.

5 Conclusions

This research finds significant and consistent geophysical effects in the low-latitude plasma drift speed data provided by IMAGE-FUV. The first effect is a reduction of zonal drift speeds with increasing D_{st}. Though not entirely unexpected, the effect is remarkably clear in the data set and reflects the strong, regular influence of electric fields originating in an energized ring current. The drift speed is controlled by a downward, polarization electric field, which must be weakened or countered by an upward electric field to slow the drifts. This could originate in asymmetric separation of charges in the energized ring current, as recently described by Ridley and Liemohn (2002).

The second interesting effect is the longitudinal variation in zonal plasma drift speeds. From observations during the two months after vernal equinox, a peak in eastward zonal plasma drift speed is found to exist between 80° and 120°E longitude. This is generally near, but not always co-located with, the maximum in the low-latitude geomagnetic field. The overall heightening of the drift speeds in this sector may be due to a generally lower pedersen conductance caused by stronger evacuation of ionospheric plasma during the daytime (resulting in stronger polarization electric fields at night), or a different distribution of ionospheric plasma, with greater proportion in the F-region. This could also be driven mainly by the dynamics of the dayside ionosphere in this region of maximum magnetic field strength. The importance of either of these possible effects cannot be decisively determined in this first report of the localized drift enhancement. Further study with in-situ data from satellites such as DMSP and NOAA and the new C-NOFS mission will help to clarify the drivers of the zonal drift enhancement in the Asian sector.

Acknowledgements. IMAGE FUV analysis is supported by NASA through Southwest Research Institute subcontract number 83 820 at the University of California, Berkeley, contract NAS5-96020.

Topical Editor M. Lester thanks I. H. Sastri and another referee for their help in evaluating this paper.

References

Aggson, T. L., Maynard, N. C., Herrero, F. A., Mayr, H. G., Brace, L. H., and Liebrecht, M. C.: Geomagnetic equatorial anomaly in zonal plasma flow, J. Geophys. Res.,92, 311–315, 1987.

Biondi, M. A., Meriwether, J. W., Fejer, B. G., Gonzales, S. A., and Hallenbeck, D. C.: Equatorial thermospheric wind changes during the solar cycle measurements at Arequipa, Peru, from 1983 to 1990, J. Geophys. Res., 96, 15 917–15 930, 1991.

Biondi, M. A., Sazykin, S. Y., Fejer, B. G., Meriwether, J. W., and Fesen, C. G.: Equatorial and low latitude thermospheric winds: measured quiet time variations with season and solar flux from 1980 to 1990, J. Geophys. Res., 104, 17 091–17 106, 1999.

Blanc, M.: Midlatitude convection electric fields and their relation to ring current development, Geophys. Res. Lett., 5, 203–206, 1978.

Blanc, M. and Richmond, A. D.: The ionospheric disturbance dynamo, J. Geophys. Res., 85, 1669–1688, 1980.

Burke, W. J. and Maynard, N. C.: Satellite observations of electric fields in the inner magnetosphere and their effects in the mid-to-low latitude ionosphere, IEEE Trans, on Plasma Sci., 28, 1903–1911, 2000.

Coley, W. R. and Heelis, R. A.: Low-latitude zonal and vertical ion drifts seen by DE 2, J. Geophys. Res., 94, 6751–6761, 1989.

Coley, W. R., Heelis, R. A., and Spencer, N. W.: Comparison of low-latitude ion and neutral zonal drifts using DE 2 data, J. Geophys. Res., 99, 341–348, 1994.

de Paula, E. R., Kantor, I. J., Sobral, J. H. A., Takahashi, H., Santana, D. C., Gobbi, D., de Medeiros, A. F., Limiro, L. A. T., Kil, H., Kintner, P. M., and Taylor, M. J.: Ionospheric irregularity zonal velocities over cachoeira paulista, J. Atmos. Solar-Terr. Phys., 64, 1511–1516, 2002.

Fejer, B. G.: F Region plasma drifts over Arecibo: Solar cycle, seasonal and magnetic activity effects, J. Geophys. Res., 98, 13 645–13 652, 1993.

Fejer, B. G.: Low latitude storm time ionospheric electrodynamics, J. Atmos. Solar-Terr. Phys., 64, 1401–1408, 2002.

Fejer, B. G. and Scherliess, L.: Mid and low-latitude prompt penetration ionospheric zonal plasma drifts, Geophys. Res. Lett., 25, 3071–3074, 1998.

Fejer, B. G., Farley, D. T., Gonzales, C. A., Woodman, R. F., and Calderon, C.: F region east-west drifts at Jicamarca, J. Geophys. Res., 86, 215–218, 1981.

Fejer, B. G., Kudeki, E., and Farley, D. T.: Equatorial F-region zonal plasma drifts, J. Geophys. Res., 90, 12 249–12 255, 1985.

Fejer, B. G., de Paula, E. R., González, S. A., and Woodman, R. F.: Average vertical and zonal F region plasma drifts over Jicamarca, J. Geophys. Res., 96, 13 901–13 906, 1991.

Fejer, B. G., de Paula, E. R., Heelis, R. A., and Hanson, W. B.: Global equatorial ionospheric vertical plasma drifts measured by the AE-E satellite, J. Geophys. Res., 100, 5769–5776, 1995.

Foster, J. C. and Rich, F. J.: Prompt midlatitude electric field effects during severe geomagnetic storms, J. Geophys. Res., 103, 26 367–26 372, 1998.

Frey, H. U., Mende, S. B., Immel, T. J., Gérard, J.-C., Hubert, B., Habraken, S., Spann, J., Gladstone, G. R., Bisikalo, D. V., and Shematovich, V. I., Summary of quantitative interpretation of IMAGE far ultraviolet auroral data, *Space Sci. Rev., 109*, 255–283, 2003.

Hedin, A. E.: Correlations between thermospheric density and temperature, solar EUV flux, and 10.7 cm flux variations, J. Geophys. Res., 89, 9828–9834, 1984.

Immel, T. J., Mende, S. B., Frey, H. U., Peticolas, L. M., and Sagawa, E.: Determination of low latitude plasma drift speeds from FUV images, Geophys. Res. Lett., 30, 1945, 2003.

Judge, D. L., McMullin, D. R., Ogawa, H. S., Hovestadt, D., Klecker, B., Hilchenbach, M., Mobius, E., Canfield, L. R., Vest, R. E., Watts, R., Tarrio, C., Kuhne, M., and Wurz, P.: First solar EUV irradiances obtained from SOHO by the CELIAS/SEM, Solar Physics, 177, 161–173, 1998.

Kamide, Y., Baumjohann, W., Daglis, I. A., Gonzalez, W. D., Grande, M., Joselyn, J. A., McPherron, R. L., Phillips, J. L., Reeves, E. G. D., Rostoker, G., Sharma, A. S., Singer, H. J., Tsurutani, B. T., and Vasyliunas, V. M.: Current understanding of magnetic storms: Storm-substorm relationships, J. Geophys. Res., 103, 17 705–17 728, 1998.

Kelley, M. C.: The earth's ionosphere plasma physics and electrodynamics, Academic Press, Inc., San Diego, 1989.

Makela, J. J., Kelley, M. C., Gonzalez, S. A., Aponte, N., and McCoy, R. P.: Ionospheric topography maps usin multiple-wavelength all-sky images, J. Geophys. Res., 106, 29 161–29 174, 2001.

Martinis, C., Eccles, J. V., Baumgardner, J., Manzano, J., and Mendillo, M.: Latitude dependence of zonal plasma drifts obtained from dual-site airglow observations, J. Geophys. Res., 108, 1129, 2003.

Maynard, N. C., Aggson, T. L., Herrero, F. A., Liebrecht, M. C., and Saba, J. L.: Average equatorial zonal and vertical ion drifts determined from San Marco D electric field measurements, J. Geophys. Res., 100, 17 465–17 479, 1995.

Mende, S. B., Heetderks, H., Frey, H. U., Stock, M., Lampton, M., Geller, S. P., Abiad, R., Siegmund, O. H. W., Habraken, S., Renotte, E., Jamar, C., Rochus, P., Gérard, J.-C., Sigler, R., and Lauche, H.: Far ultraviolet imaging from the IMAGE spacecraft. 3. Spectral imaging of Lyman-α and OI 135.6 nm, Space Sci. Rev., 91, 287–318, 2000.

Mendillo, M. and Baumgardner, J.: Airglow characteristics of equatorial plasma depletions, J. Geophys. Res., 87, 7641–7652, 1982.

Meriwether, J. W., Biondi, M. A., and Anderson, D. N.: Equatorial airglow depletions induced by thermospheric winds, Geophys. Res. Lett., 12, 487–490, 1985.

Pimenta, A. A., Bittencourt, J. A., Fagundes, P. R., Sahai, Y., Buriti, R. A., Takahashi, H., and Taylor, M. J., Ionospheric plasma bubble zonal drifts over the tropical region: a study using OI 630nm emission all-sky images, J. Atmos. Solar-Terr. Phys., 65, 1117–1126, 2003.

Ridley, A. J. and Liemohn, M. W.: A model-derived storm time asymmetric ring current driven electric field description, J. Geophys. Res., 107, SMP–2, 2002.

Sagawa, E., Maruyama, T., Immel, T. J., Frey, H. U., and Mende, S. B.: Global view of the nighttime low latitude ionosphere by the 135.6 nm OI observation with IMAGE/FUV, Geophys. Res. Lett., 30, 1534–1537, 2003.

Scherliess, L. and Fejer, B. G.: Storm time dependence of equatorial disturbance dynamo zonal electric fields, J. Geophys. Res., 102, 24 037–24 046, 1997.

Scherliess, L. and Fejer, B. G.: Satellite studies of mid- and low-latitude ionospheric disturbance zonal plasma drifts, Geophys. Res. Lett., 25, 1503–1506, 1998.

Sobral, J. and Abdu, M.: Solar activity effects on equatorial plasma bubble zonal velocity and its latitude gradient as measured by airglow scanning photometers, J. Atmos. Terr. Phys., 53, 729–742, 1991.

Sobral, J. H. A., Abdu, M. A., Takahashi, H., Sawant, H., Zamlutti, D., and Borba, G. L.: Solar and geomagnetic activity effects on nocturnal zonal velocities of ionospheric plasma depletions, Advances in Space Research, 24, 1507–1510, 1999.

Tanaka, T.: Low-latitude ionospheric disturbances: Results for 22 March, 1979, and their general characteristics, Geophys. Res. Lett., 13, 1399–1402, 1986.

Taylor, M. J., Eccles, J. V., LaBelle, J., and Sobral, J. H. A.: High resolution OI (630 nm) image measurements of F-region depletion drifts during the Guara campaign, Geophys. Res. Lett., 24, 1699–1702, 1997.

Valladares, C. E., Sheehan, R., Basu, S., Kuenzler, H., and Espinoza, J.: The multi-instrumented studies of equatorial thermosphere aeronomy scintillation system: Climatology of zonal drifts, J. Geophys. Res., 101, 26 839–26 850, 1996.

Weber, E. J., Buchau, J., Eather, R. H., and Mende, S. B.: North-south aligned equatorial airglow depletions, J. Geophys. Res., 83, 712–716, 1978.

Woodman, R. F.: East-west ionospheric drifts at the magnetic equator, Space Res., 81, 5447–5466, 1972.